Paper #070EN-0372 **Topic: Environmental Aspects of Combustion**

8th U. S. National Combustion Meeting
Organized by the Western States Section of the Combustion Institute
and hosted by the University of Utah
May 19-22, 2013

Effect of Unsaturated Bond on PAH and Soot Formation in n-Heptane and 1-Heptene Partially Premixed Flames

Xiao Fu, Xu Han, and Suresh K. Aggarwal

Department of Mechanical & Industrial Engineering, University of Illinois at Chicago, 842 W. Taylor Street, Chicago, IL 60607, USA

Previous studies have demonstrated that the presence of unsaturated bonds in the fuel molecular structure can significantly influence the fuel reactivity, and thereby its ignition, combustion, and emission characteristics. We report herein a numerical investigation on the structure and emissions characteristics of partially premixed flames burning n-heptane and 1-heptene fuels. Our objective is to examine the effect of unsaturated (double) bond on PAH and soot emissions in a flame environment containing regions of rich premixed and nonpremixed combustion. A validated detailed kinetic model with 198 species and 4932 reactions was used to simulate partially premixed flames in a counterflow configuration with different levels of premixing and strain rates. The soot processes including nucleation, surface reactions, and coagulation are modeled using the Frenklach's method of moments approach. Results indicate that although the global structures of n-heptane and 1-heptene partially premixed flames are quite similar, there are significant differences with respect to polycyclic aromatic hydrocarbon (PAH) and soot emissions from these flames. The PAH species are mainly formed in the rich premixed zone, and their emissions are significantly higher in 1-heptene flames than in n-heptane flames. The reaction pathway analysis indicated that the dominant path for benzene formation involves the recombination of two propargyl radicals (C_3H_3), and the presence of the double bond in 1-heptene provides a significant route for its production through the formation of allyl radical (C_3H_5). This path is not favored in the oxidation of n-heptane, as it decomposes directly to smaller alkyl radicals. For both the fuels, the nucleation process is initiated in the rich premixed zone in which there is abundance of PAH species. However, most of soot is formed in the region between the two reaction zones. More importantly, the amount of soot formed in 1-heptene flames is significantly higher than that in n-heptane flames. As the partially premixing level is decreased, the soot particle number density, particle diameter and soot volume fraction are increased for both n-heptane and 1-heptene fuels. The differences between the two fuels in terms of both the size and the number of soot particles are increased as the partially premixing level is decreased. While the PAH and soot emissions decrease with the increase in strain rate, these are consistently higher in 1-heptene flames than in n-heptane flames, irrespective of the strain rate.

1. Introduction

There is significant interest in using biodiesel fuels in transport applications, as these fuels can be produced from a variety of renewable resources, and have lower emissions compared to petroleum diesel. Their chemical composition and properties vary over a wide range depending upon the sources and processes used to make the biofuels. An important characteristic of biodiesels, produced via the esterification of vegetable oils and animal fat, is the existence of double and triple bonds in their molecular structure. The chain length and unsaturated bonds in the fuel molecular structure are known to have a significant influence on the fuel combustion chemistry and, thereby, on the combustion characteristics, including ignition delay, flame speed, and pollutant emissions.

Diesel engine experiments performed by Lapuerta et al. [1] using waste cooking oil biodiesel, indicated noticeable reductions in particulate matter (PM) emissions with the decrease in the number

of double bonds or degree of unsaturation in the fuel molecular structure. Puhan et al. [2] reported increased emissions of NO_x, smoke, CO, and unburned hydrocarbons (UHCs) with the increase in the degree of unsaturation, on the basis of their single-cylinder engine experiments with linseed, jatropha, and coconut oils. Schönborn et al. [3] reported higher PM emissions with the increase in the number of double bonds for fatty acid alkyl esters obtained from vegetable oils via transesterification. Benjumea et al. [4] conducted single-cylinder engine experiments with three different mixtures of fatty acid methyl esters and showed that smoke opacity and emissions of NO_x and UHCs increased with the degree of unsaturation. In addition, a higher degree of unsaturation was found to increase the ignition delay and retard the start of combustion, which is also expected to influence the PM and NO_x emissions. Salamanca et al. [5] examined the effects of chemical composition and the degree of unsaturation of methyl esters on engine emissions and observed that linseed biodiesel produced more PM and UHCs than palm biodiesel as a consequence of more unsaturated compounds in its composition, which favor the formation of soot precursors. In summary, previous engine studies show that unsaturation components in biodiesel fuels lead to increased PM emissions.

In order to explain this trend in PM emissions from diesel engines, there have been fundamental studies on the formation of PAHs and soot precursors from the combustion of biodiesel components. One of the major routes for PAH formation and soot particle surface growth is through "H-abstraction-C_2H_2-addition" (HACA) reactions, which are driven by C_2H_2 [6,7]. Garner et al. [8] performed shock tube pyrolysis experiments using n-heptane (n-C_7H_{16}) and 1-heptene (1-C_7H_{14}) as analogs for the saturated and unsaturated hydrocarbon side chains of C_8 methyl esters, and observed that 1-heptene produces more acetylene than does the n-C_7H_{16} over intermediate temperatures, 1100-1600K. Sarathy at el. [9] compared two fatty acid methyl esters, methyl butanoate ($C_3H_7COOCH_3$) and its unsaturated counterpart methyl crotonate ($CH_3CH=CHCOOCH_3$), in counterflow diffusion flame and jet stirred reactor. Methyl crotonate was observed to produce higher amount of C_2H_2, 1-C_3H_4, 1-C_4H_8, 1,3-C_4H_6, and benzene, indicating the potential of increased soot formation with unsaturated biodiesel fuels compared to the saturated ones, although soot emission is reduced with biodiesel compared to petroleum diesel due to the presence of oxygen in biodiesel and the significantly higher amount of aromatics in petroleum diesel. Our previous studies on n-C_7H_{16} and 1-C_7H_{14} partially premixed counterflow flames (PPFs) [10, 11] revealed that unsaturated fuel, 1-C_7H_{14} produces higher amount of C_2H_2 and benzene compared to the saturated fuel, n-C_7H_{16}.

The present work extends our previous investigation, and examines the effect of the presence of a double bond on both PAHs and soot formation in PPFs burning prevaporized n-C_7H_{16} and 1-C_7H_{14} fuels. Since these fuels represent the hydrocarbon side chain of the saturated and unsaturated methyl esters, namely methyl octanoate and methyl *trans*-2-octenoate, the study is also relevant to the understanding of soot emissions from the combustion of biodiesel fuels. Another objective is to characterize the soot formation processes in a flame environment containing regions of both rich premixed and non-premixed combustion, for which relatively little research has been reported. The PPFs have been simulated in an opposed jet flow configuration because of its simple flow field and its relevance to diesel engine combustion [12]. The soot processes considered include the particle nucleation, surface growth and oxidation, and coagulation, and are modeled using the Frenklach's method of moments approach. The soot model is combined with a detailed fuel oxidation model involving 198 species and 4932 reactions. The combined model is validated using soot measurements n-heptane PPFs [13] and soot measurements in ethylene diffusion flames [14]. Simulations are performed to characterize the effects of double bond on PAH and soot emissions for a range of equivalence ratios and strain rates.

2. The Physical-Numerical Model

The counterflow flame configuration employed in the present investigation is shown schematically in Figure 1. It consists of two opposing jets issuing from two coaxial nozzles that are placed one above the other. A rich fuel-air mixture flows from the lower nozzle and air from the upper nozzle. The separation distance between the nozzles is 1.5cm in this study. Fuel inlet temperature is kept at 400K while oxidizer temperature at 300K. PPFs are established for the two fuels by independently varying the fuel stream equivalence ratio (ϕ) and the global strain rate, a_G, [15] which is expressed as

$$a_G = \frac{2v_o}{L}\left(1+\frac{v_f\sqrt{\rho_f}}{v_o\sqrt{\rho_o}}\right) \tag{1}$$

Here L denotes the separation distance between the two jets, v_f the fuel jet inlet velocity, v_o the oxidizer jet inlet velocity, and ρ_f and ρ_o the mixture densities in the fuel and oxidizer streams, respectively. The inlet velocities of the fuel and oxidizer streams are specified by matching the momentum of the two streams for given ϕ and a_G. For this investigation, the strain rate was varied from 50^{-1} to $350s^{-1}$. At higher strain rate, $a_G > 350s^{-1}$, the amount of soot formed was relatively small due to the short resident time.

Simulations were performed using the OPPDIF from CHEMKIN Pro 15101 packages [13, 16]. The kinetic mechanism used to model n-heptane and 1-heptene flames has been developed previously by extending a detailed oxidation scheme for several fuels [17,18]. Due to the hierarchical modularity of the mechanistic scheme, the model is based on a detailed sub-mechanism of C_1 - C_4 species. Investigation on the formation of the first aromatic rings by C_2 and C_4 chemistry and by resonance-stabilized radicals such as propargyl and allyl has been performed by Goldaniga et al. [18]. The NO_x mechanism was adopted from various sources. Thermal [19], prompt [20], intermediate N_2O [21], and NNH [22] mechanisms are included from various sources. Details regarding these mechanisms have been discussed in a previous investigation [10].

Figure 2 presents a schematic of the soot formation processes [23]. As fuel molecules begin to decompose, intermediate hydrocarbon species are formed in fuel rich regions, which undergo further reactions to form PAHs. Once the primary particle is formed through nucleation and polymerization, it can grow through surface reactions and coagulation, and also undergo oxidation. The kinetic model used for fuel oxidation is capable of simulating the formation of PAHs up to pyrene ($C_{16}H_{10}$). Particle inception is modeled by a nucleation reaction with two pyrene molecules as the reactants. The nucleation reaction is an irreversible reaction which provides the particle inception rate and defines the size and the surface coverage of the particle (or nucleus). The nuclei start to interact with each other through coagulation as well as with the gaseous species on its surface. The dynamics of coagulation can be modeled by solving particle size distribution functions (PSDFs). To solve PSDFs, either a discrete-sectional method [24] or the method of moments [7] can be used. Although reasonably accurate, discrete methods are known to be computationally very expensive and are not considered here. Instead, the method of moment employed by Frenklach [25,26] is used to describe the moments of the PSDFs. The results reflect the average properties of soot population without a priori knowledge of PSDF; therefore require dramatically less computational resources. The soot formation model also includes surface reactions with gaseous species to determine the surface growth and oxidation rates [25]. The soot aggregation process is not considered in the present study. Numerical simulations are performed to examine the effects of strain rate, equivalence ratio and fuel molecular structure on PAH and soot emissions.

3. Results and Discussion

Model Validation

While the present kinetic mechanism for fuel oxidation has been extensively validated in previous studies, we provide an additional validation here using the measurements of Berta et al. [13, 27] for an n-heptane PPF established at $\phi = 4.27$, $a_G = 100s^{-1}$, and nitrogen dilution of 17%. Figure 3 presents the predicted and measured mole fraction profiles for several hydrocarbon species including a PAH species, benzene. There is a good qualitative agreement between predictions and measurements, especially with respect to intermediate hydrocarbon (C_2H_2, C_2H_4 and CH_4) species profiles. However, the peak benzene mole fraction is overpredicted by about 25% compared to measurements. The comparison for four other flames found this discrepancy in the predicted peak benzene mole fraction to be from 20% to 30%. [13]

A validation of the soot model is presented in Figure 4, which presents a comparison of predictions with the experimental measurements of soot volume fractions reported by Hwang and Chung [14] and Vansburger et al. [28] in a counterflow ethylene diffusion flame. For these results, the separation distance between the fuel and oxidizer nozzles was 1.42cm, and the exit velocities of both fuel and oxidizer streams were 19.5cm/s. Results are shown for two different compositions of the oxidizer stream, namely 20% O_2 + 80% N_2 and 24% O_2 + 76% N_2 by volume. The fuel stream contained pure C_2H_4. There is good agreement between the predictions and measurements for the 20% O_2 case. However, the numerical model overpredicts the soot volume fractions by a factor of 2 compared to measurements for the 24% O_2 case. Similar discrepancy has been reported by Liu et al. [29], who attributed it to the lack of information on the correct experimental conditions including the boundary conditions. Moreover, their two-equation soot model was originally optimized for premix flames. Consequently, Liu et al. used a larger nozzle separation distance of 1.7cm, and reduced the surface growth rate in their model by a factor of 2.5 in order to achieve agreement with the measurements of Hwang and Chung [14]. Since the soot model in the present study has also been optimized for premixed flames [7], the overprediction of soot volume fraction by a factor of 2 is seemed acceptable.

Structure of n-Heptane and 1-Heptene Partially Premixed Flames

In order to gain insight into the effect of unsaturated bond on soot formation and oxidation processes, the structures of partially premixed flames for n-heptane and 1-heptene fuels are presented in Figure 5. The strain rate is $a_G = 50s^{-1}$, and ϕ in the fuel stream is 2, with 17% nitrogen dilution. The oxidizer stream is pure air at a temperature of 300K, while the fuel stream temperature is 400K, since the fuel is considered in the gaseous form. In each figure, several gaseous and soot properties are shown. The gaseous properties include profiles of temperature, axial velocity, heat release rate (HRR), and mole fractions of acetylene and pyrene. The soot properties include the average particle diameter, particle number density and soot volume fraction plotted versus the distance from the fuel nozzle. The stagnation plane location is indicated by the vertical line. The global flame structures for the two fuels are quite similar, implying that the overall combustion process is not strongly influenced by the presence of the unsaturated bond. For both fuels, the HRR profile contains two peaks, one corresponding to the rich premixed reaction zone located on the fuel side and the other indicating the nonpremixed reaction zone located close to the stagnation plane. The hydrocarbon species profiles indicate that C_2H_2 and PAHs are formed in the rich premixed zone, while the peak temperature occurs in the nonpremixed reaction zone, where most of H_2O and CO_2 are produced. The peak in pyrene mole fraction is located downstream of the peak in C_2H_2 mole

fraction. The particle number density profile indicates that the nucleation is initiated with the formation of PAH species. Subsequently, the particle diameter and soot volume fraction increase due to surface reactions and coagulation, while the number density is determined by a competition between the nucleation and coagulation processes. The peaks in particle diameter and soot volume fraction are located near the stagnation plane (on the fuel side), where the pyrene mole fraction decreases to zero. Clearly there is little soot oxidation in the region between the rich premixed and nonpremixed reaction zones, due to the lack of oxygen in this region. Both the number density and soot volume fraction become zero right after crossing the stagnation plane. However, the average particle diameter becomes zero at some finite distance from the stagnation plane, suggesting that only a small amount of soot diffuses to the oxidizer side and is oxidized.

Effect of Fuel Molecular Structure on PAH and Soot Emissions

As discussed in previous studies [9, 10, 11], unsaturated fuels produce higher amounts of hydrocarbons, such as C_2H_2, C_3H_3, and C_6H_6, which result in higher amounts of PAHs and soot. This is supported by the simulation results presented in Figure 5, indicating significantly higher concentration of pyrene in 1-heptene flame compared to that in n-heptane flame. As a consequence, the soot diameter, number density, and volume fraction are also higher in 1-heptene flame compared to those in n-heptane flame, and the differences are related to the presence of the double bond in 1-heptene. The effect of double bond on PAH and soot emissions is further illustrated in Figures 6-8. Figure 6 presents the peak mole fractions of benzene and pyrene plotted versus strain rate in n-heptane and 1-heptene PPFs at ϕ=2 and 8. As expected, as the strain rate is decreased and/or the level of premixing is reduced (i.e., ϕ is increased), the peak benzene and pyrene concentrations decrease. More importantly, significantly higher amounts of these species are formed in 1-heptene flames than in n-heptane flames. As a consequence, the amount of soot formed is also noticeably higher in 1-heptene flames. As depicted in Figure 7, both the soot number density and volume fraction are much higher in 1-heptene flames compared to those in n-heptane flames. Similarly, the average soot particle diameter is higher in 1-heptene flames, as shown in Figure 8. Again the effect of increased partial premixing and strain rate is to reduce the amount of soot formed in partially premixed flames.

The differences in the particle number density and volume fraction can be related to the nucleation process, which is based on pyrene concentration, and to the surface growth due to surface reactions and coagulation processes. The nucleation model in the present soot mechanism is

$$2\ C_{16}H_{10} \Rightarrow 32\ C + 20\ C_{soot}\text{-}H + 28.75\ C_{soot}\bullet \qquad \text{(R2)}$$

In this reaction, two pyrene molecules combine to form one soot nucleus containing 32 C atoms. The C_{soot}-H is a carbon atom site with surface-bonded hydrogen atom, while the C_{soot}• is an open (or empty) surface site. The surface site density is defined as the number of active chemical sites per surface area where adsorption, desorption, and chemical reaction can take place. Here 20 of the C atoms have H surface sites and about 28.75 of the 32 C atoms are open sites. The C_{soot}-H and C_{soot}• sites then react with gaseous species through surface growth reactions R3-R8.

So the increasing difference in soot particle diameter at higher ϕ is due to higher soot particle population and surface growth rate. As discussed by Frenklach [26], the coagulation rate is based on Smoluchowski's theory of Brownian motion [24] and is proportional to the square of total particle number of the population. Thus a higher ϕ leads to increased coagulation rate due to larger population of particles. In addition, as ϕ is increased, soot surface growth rate also becomes

significantly higher in 1-heptane flame compared to that in n-heptane flame. Surface growth is modeled through the HACA mechanism, represented by the following reactions:

$$H + C_{soot}\text{-}H \Rightarrow C_{soot}\bullet + H_2 \quad \text{(R3)}$$

$$C_{soot}\bullet + H_2 \Rightarrow C_{soot}\text{-}H + H \quad \text{(R4)}$$

$$C_{soot}\bullet + H \Rightarrow C_{soot}\text{-}H \quad \text{(R5)}$$

$$C_{soot}\text{-}H + OH \Rightarrow H_2O + C_{soot}\bullet \quad \text{(R6)}$$

$$H_2O + C_{soot}\bullet \Rightarrow OH + C_{soot}\text{-}H \quad \text{(R7)}$$

$$C_{soot}\bullet + C_2H_2 \Rightarrow C_{soot}\text{-}H + 2C + H \quad \text{(R8)}$$

As indicated, C_2H_2, H and OH are the main reacting species in this mechanism. In reaction R8, a C_2H_2 molecule attaches to the $C_{soot}\bullet$ site and forms C_{soot}-H and H. In addition, two carbons are added to the carbon bulk. As reported in previous studies [10, 11] an increase in ϕ leads to higher C_2H_2 concentration, and since more C_2H_2 is formed in 1-heptene flames than that in n-heptane flames, it leads to significantly higher surface growth rate in 1-heptene flames.

In order to gain further insight into the effect of double bond on PAH and C_2H_2 formation, reaction pathway analyses were performed, and results are summarized in Figure 9 (a) and (b), which present the dominant pathways for the formation of benzene in n-heptane and 1-heptene flames, respectively. While the oxidation of these two fuels follows different paths depending upon the temperature, benzene is mainly formed through the recombination reaction of propargyl radicals (C_3H_3) [30]. Most of C_3H_3 is formed from allyl radicals (C_3H_5), and the formation of allyl from fuel decomposition is quite different for n-heptane and 1-heptene fuels, as can be seen on the left side of Figure 9 (a) and (b). At high temperatures (>1200K), typical of flame environment, most of 1-heptene directly decomposes into C_3H_5 and C_4H_9. In contrast, the decomposition of n-heptane at high temperature mostly involves C-C bond fission, forming various alkyl radicals, such as CH_3, C_6H_{13}, C_2H_5, C_5H_{11}, C_3H_7 and C_4H_9, most of which then decompose into C_2H_4 and CH_3 (not shown) through β scission and H abstraction (H abs.) reactions. Similarly, the butyl (C_4H_9) formed from 1-heptene also decomposes into C_2H_4. In fact, this is the main source of ethylene in 1-heptene flame (cf. Figure 9b), while there are multiple alkyl species (C_6H_{13}, C_5H_{11}, C_4H_9, C_3H_7, etc.) that form ethylene in n-heptane flame (cf. Figure 9a). Consequently, the ethylene concentration is higher in n-heptane flame compared to that in 1-heptene flame. Ethylene subsequently forms vinyl (C_2H_3), which can also produce benzene through its reaction with butadiene. However, the higher C_2H_4 concentration does not imply increased benzene production in n-heptane flame, since the butadiene concentration is much lower in this flame compared to that in 1-heptene flame. This aspect is further discussed in the following.

As indicated in Figure 9, the low-temperature (<1200K) oxidation paths of n-alkane and 1-alkene are also significantly different. The decomposition of n-heptane is initiated by H abstraction forming n-alkyl radicals, which then break into various 1-alkenes (C_3H_6, C_4H_8, C_5H_{10}) and smaller alkyls (CH_3, to C_5H_{11}) through β-scission and H abstraction reactions. The smaller alkyls subsequently form C_2H_4, which lead to the production of benzene through vinyl (C_2H_3), similar to the high-temperature reaction path discussed above. The various 1-alkanes (except C_2H_4) on the other hand represent the main source of allyl and butadiene, which subsequently form benzene. However, the formation of allyl competes with that of butadiene in n-heptane flames, unlike the case for 1-heptene flames (discussed below), in which the path to butadiene is preferred. Consequently, the amount of butadiene formed in n-heptane flames is significantly lower than that in 1-heptene flames. The low-temperature oxidation of 1-heptene follows three different paths. The main path involves H abstraction at the alpha-carbon location near the double bond, forming 1-butylallyl radicals, which

then break into 1,3-butadiene and propyl. The second path involves H addition and formation of n-C7 alkyl radicals, which then follow a similar path as that for n-heptane discussed above. The third path involves the decomposition of 1-heptene through H abstraction from other C-H bonds, forming other 1-C_7H_{13} radicals, which then form propargyl (though allyl) and 1-C_4H_7, and subsequently benzene. In summary, for the low-temperature reaction path, n-heptane tends to produce more allyl than 1-heptene. However, in the rich premixed flame environment, the benzene formation is dominated by the high-temperature reaction path, with the implication that significantly higher amount of benzene is formed in 1-heptene flames compared to that in n-heptane flames. The above pathway from fuel to benzene formation as well as the observations regarding the importance of allylic radicals, propargyl, vinyl, and 1,3-butadiene (C_4H_6) are consistent with previous studies; see, for example Zhang et al. [31], who examined the chemistry of aromatic precursor formation in n-heptane premixed flames. Note, however, that the high-temperature reaction pathway was found to be more important for benzene formation in our study.

Finally, it should be mentioned that C_2H_2 is known to be an important precursor for PAH and soot production. As stated earlier, the presence of double bond leads to the higher production of C_2H_2 in 1-heptene flames than in n-heptane flames. In the context of Figure 9, C_2H_2 is mainly formed from vinyl, and produces benzene through its reaction with C_4H_5 radicals, which are formed from butadiene. Acetylene subsequently plays an important role in the formation of larger PAH species through the HACA mechanism as discussed above. It is also important to note that the concentration of C_2H_4 is higher in n-heptane flames, while that of C_2H_2 is higher in 1-heptene flames. This is due to the fact that C_2H_2 is produced from both C_2H_4 (through vinyl) and C_4H_5 (which breaks down to form C_2H_2 and C_2H_3), and the concentration of C_4H_5 is noticeably higher in 1-heptene flames, leading to the increased production of C_2H_2 in these flames.

4. Conclusions

Partially premixed flames with n-heptane and 1-heptene fuels have been simulated in a counterflow configuration in order to examine the effect of unsaturated (double) bond on PAH and soot emissions. The study is also relevant to biodiesel surrogates, as n-heptane and 1-heptene, respectively, represent the hydrocarbon side chain of the methyl-octanoate and methyl *trans*-2-octenoate. The kinetic model has been validated using previously reported measurements of n-C_7H_{16} PPFs and C_2H_4 diffusion flames. The soot emissions for the two fuels are characterized in terms of the average particle diameter, particle number density and soot volume fraction at different partial premixing levels and strain rates. Important observations are as follows.

Although the global structures of n-heptane and 1-heptene partially premixed flames are generally similar, there are significant differences with respect to PAHs and soot emissions between these flames. The PAH species are mainly formed in the rich premixed zone; and their emissions are significantly higher in 1-heptene flames than in n-heptane flames. The reaction pathway analysis indicated that the dominant path for benzene formation involves the recombination of two propargyl (C_3H_3) radicals, and the presence of the double bond in 1-heptene provides a significant route for its production through the formation of C_3H_5. This path is not favored in the oxidation of n-heptane, as it decomposes directly to smaller alkyl radicals.

For both the fuels, the nucleation process is initiated in the rich premixed zone in which there is abundance of PAH species. However, most of soot is formed in the region between the two reaction zones. More importantly, the amount of soot formed in 1-heptene flames is significantly higher than

that in n-heptane flames. As the partially premixing level is decreased, the soot particle number density, particle diameter and soot volume fraction are increased for both n-heptane and 1-heptene fuels. The differences between the two fuels in terms of both the size and the number of soot particles are increased as the partially premixing level is decreased. While the PAH and soot emissions decrease with the increase in strain rate, these are consistently higher in 1-heptene flames than in n-heptane flames, irrespective of the strain rate

PAH species and soot emissions decrease as the strain rate is increased because of the lower residence time. The differences in soot emissions, especially in soot number density and volume fraction, due to the presence of double bond also become less pronounced at high strain rates. As the partially premixing level is decreased, or the equivalence ratio is increased, the PAHs and soot emissions become noticeably higher for both n-heptane and 1-heptene fuels. The differences in PAHs and soot emissions due to the unsaturation of the fuel also become significantly more pronounced as the level of partially premixing is decreased.

Future work will focus on performing experiments and simulations of these flames using long chain saturated and unsaturated biodiesel components for a range of equivalence ratio and strain rate.

References

[1] Lapuerta M.; Herreros J. M.; Lyons L. L.; García-Contreras R.; Briceño Y. *Fuel*. 2008, 87: 3161 3169.
[2] Puhan, S.; Saravanan, N.; Nagarajan, G.; Vedaraman, N. *Biomass Bioenergy*. 2010, 34: 1079-1088.
[3] Schönborn, A.; Ladommatos, N.; Williams, J.; Allan, R.; Rogerson, J. *Combust. Flame*. 2009, 156: 1396-1412.
[4] Benjumea, P.; Agudelo, J. R.; Agudelo, A. F. *Energy Fuels*. 2011, 25: 77-85.
[5] Salamanca, M.; Mondragon, F.; Agudelo, J. R.; Benjumea, P.; Santamaría, A. *Combust. Flame*. 2012, 159: 1100-1108.
[6] Frenklach M.; Wang H. *Proc. Combust. Inst*. 1991, 23: 1559.
[7] Frenklach M. *Phys. Chem. Chem. Phys*. 2002, 4: 2028-2037.
[8] Garner, S.; Sivaramakrishnan, R.; Brezinsky, K. *Proc. Combust. Inst*. 2009, 32: 461-467.
[9] Sarathy, S. M.; Gaïl, S.; Syed, S. A.; Thomson, M. J.; Dagaut, P. *Proc. Combust. Inst.* 2007, 31: 1015-1022.
[10] Fu X.; Garner S.; Aggarwal S. K.; and Brezinsky K. Energy Fuels. 2012, 26: 879-888.
[11] Han X.; Aggarwal S. K.; and Brezinsky K. Energy Fuels. 2013, 27: 537-548.
[12] Domingo P.; Vervisch L. *Symposium on Combustion*. 1996, 26: 233-240.
[13] Berta P. Numerical and experimental investigation of n-heptane combustion in a counterflow configuration. Ph.D. Thesis, University of Illinois at Chicago, US, 2005.
[14] Hwang J. Y.; Chung S. H. *Combust. Flame*. 2001, 125: 752-62.
[15] Fisher E. M.; Williams B. A.; Fleming J. W. Proc. *Eastern States Section Combus. Inst*. 1997, 191-194.
[16] Lutz A. E.; Kee R. J.; Grcar J. F.; Rupley F. M.. OPPDIF: a FORTRAN program for computing opposed flow diffusion flames. Technical Report SAND. 1997, 96-8243, UC-1404.
[17] Ranzi E.; Dente M.; Goldaniga A.; Bozzano G.; Faravelli T. *Progress in Energy and Combustion Science*. 2001, 27: 99.
[18] Goldaniga; Faravelli T.; Ranzi E. *Combust. Flame*. 2000, 122: 350-358.
[19] Zeldovich J. *Acta Physicochimica, U.R.S.S.* 1946, 21: 577-628.
[20] Glarborg P.; Jensen A. D.; Johnsson J. E. *Progress in Energy and Combustion Science*. 2003, 29: 89-113.
[21] Malte P.; Pratt D. T. *Proc. Combust. Inst*. 1974, 15: 1061-1070.
[22] Guo, H.; Smallwood, G. J. *Combustion Theory and Modeling*. 2007, 11: 741-753.
[23] Johnsson J.; Olofsson N. ; Bladh H.; Bengtsson P. Lund University. http://www.forbrf.lth.se/english/research/measurement_methods/laser_induced_incandescence_lii/ (accessed Jan 24, 2013).
[24] Smoluchowski M.V.; *Phys Z. Chem*. 1917, 92: 129-139.
[25] Appel J.; Bockhorn H.; Frenklach M. *Combust. Flame*. 2000, 121: 122-136.

[26] Frenklach M. and Harris S. *J. J. of Colloid and Interface Sci*. 1987, 118: 252-261.
[27] Berta P.; Aggarwal S. K.; Puri I. K. *Combust. Flame*. 2006, 145: 740-764.
[28] Vandsburger U.; Kennedy I.; Glassman I. *Combustion Science and Technology*. 1984, 39: 263-85.
[29] Liu F.; Guo H.; Smallwood G.; Hafi M. *Journal of Quantitative Spectroscopy & Radiative Transfer*. 2004, 84: 501-511.
[30] Miller, J.A.; Melius, C.F. *Combust. Flame*. 1992, 91: 21-39.
[31] Zhang, R.H.; Eddings, E.G.; Sarofim. A.F. *Energy Fuels*. 2008, 22: 945-953.

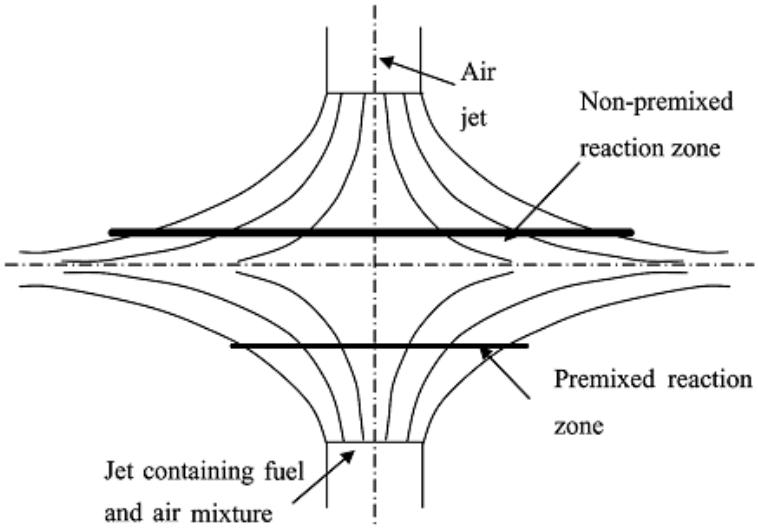

Figure 1: A schematic of the opposed jet partially premixed flame configuration.

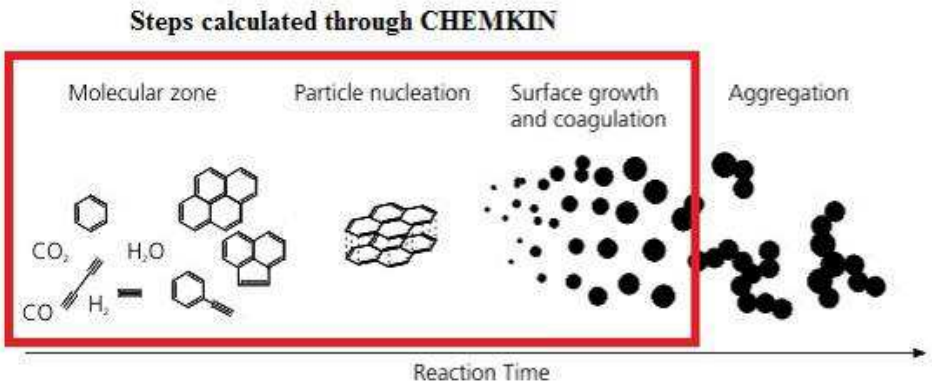

Figure 2: Soot formation process. Red box indicates the formation processes considered in current model.

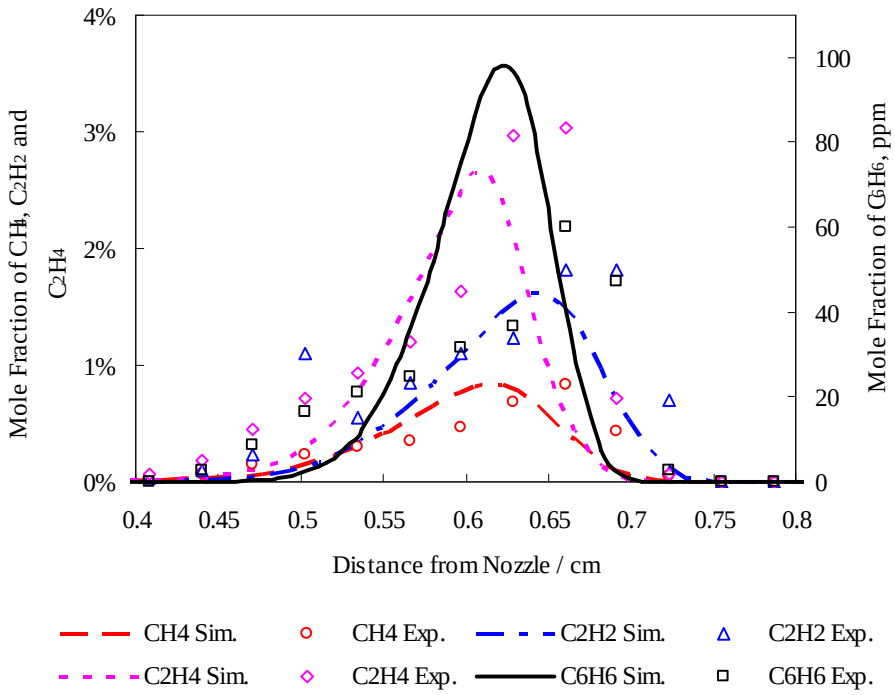

Figure 3: Predicted (lines) and measured [13] (symbols) flame structures in terms of species mole fraction profiles for n-heptane partially premixed flame at $\phi = 4.27$, $a_G = 100s^{-1}$, and nitrogen dilution of 17%, which contains CH_4 (○), C_2H_2 (△), C_2H_4 (◊) and C_6H_6 (□) profiles.

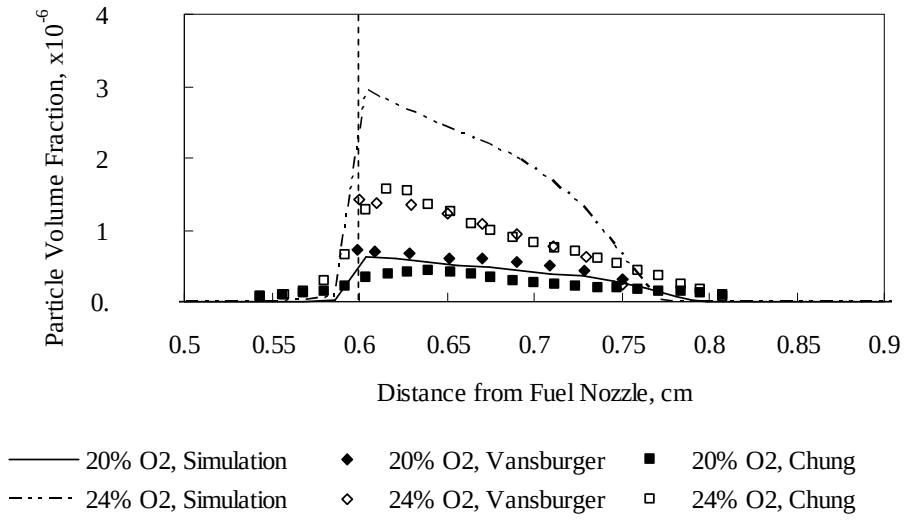

Figure 4: Predicted (lines) and measured (symbols) soot volume fraction profiles for pure C_2H_4 diffusion flame. Fuel and oxidizer nozzle exit velocities are both 19.5 cm/s. Nozzle separation length is 1.42 cm. (□) symbol is experiment data from Vansburger et al. [28] (◊) symbol is experimental data from Hwang and Chung [14]. The mole fraction of O_2 in oxidizer stream is 20% and 24%. Vertical line represents the stagnation plane.

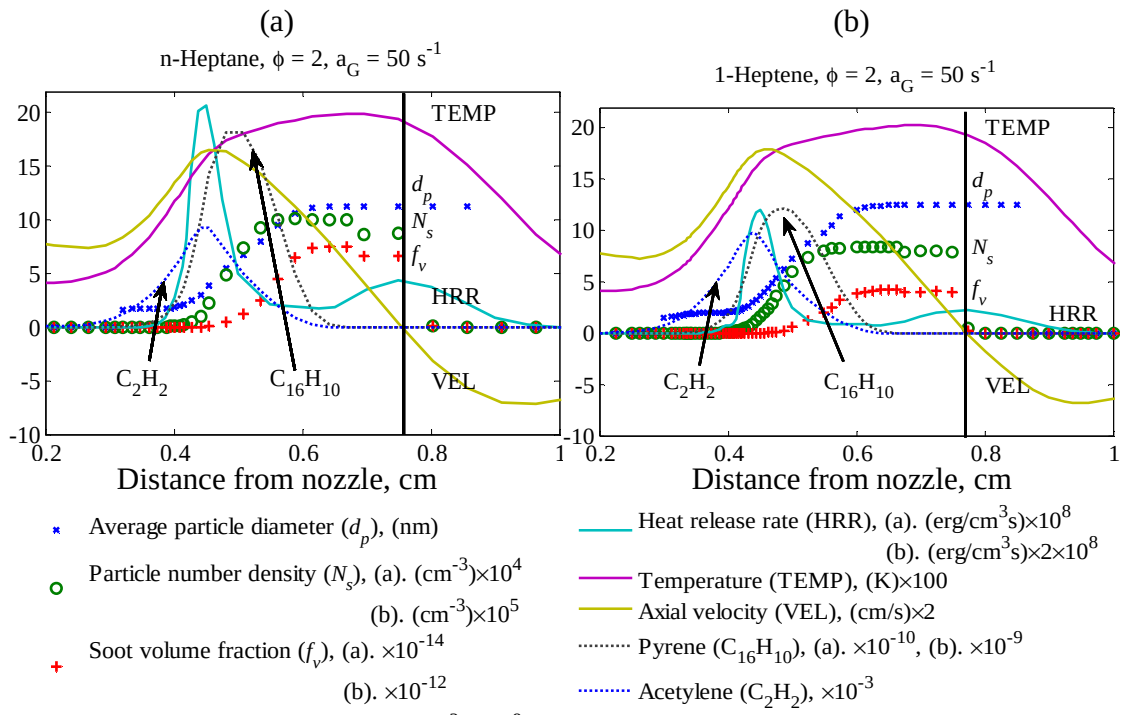

Figure 5: Flame structure of n-heptane and 1-heptene PPFs at ϕ = 2, a_G = 50s^{-1}. Dotted symbols are soot properties, which include average particle diameter (d_p), particle number density (N_s) and soot volume fraction (f_v). Solid lines include temperature, heat release rate and axial velocity. Dashed lines represent pyrene and acetylene mole fractions. Vertical line represents the stagnation plane.

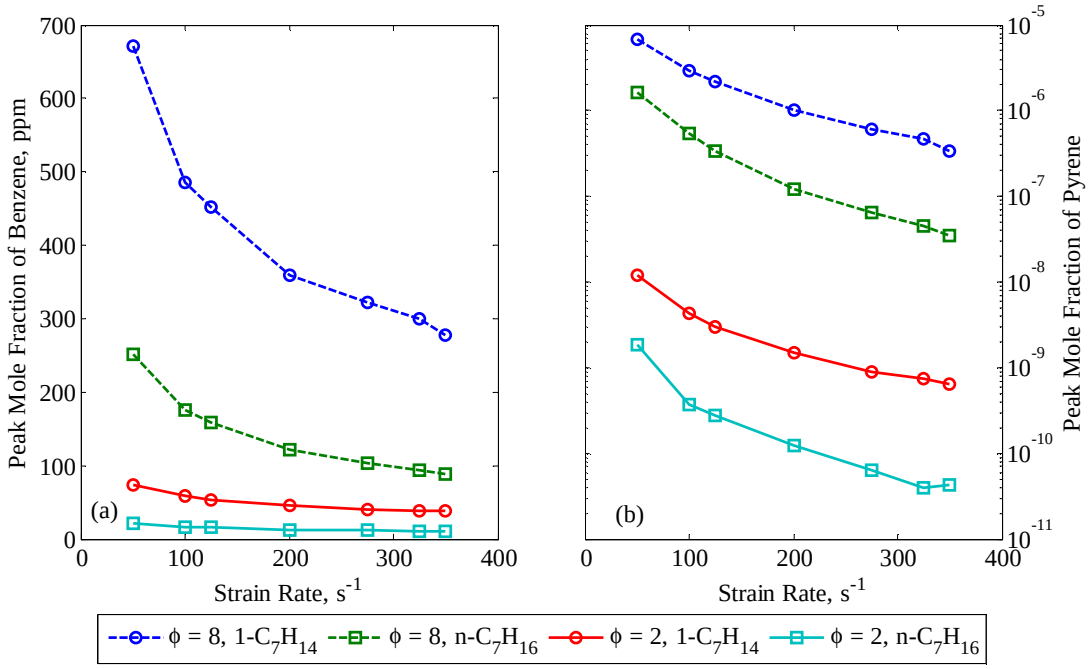

Figure 6: The peak mole fractions of benzene and pyrene plotted versus strain rate for n-heptane and 1-heptene PPFs at $\phi = 2$ and 8.

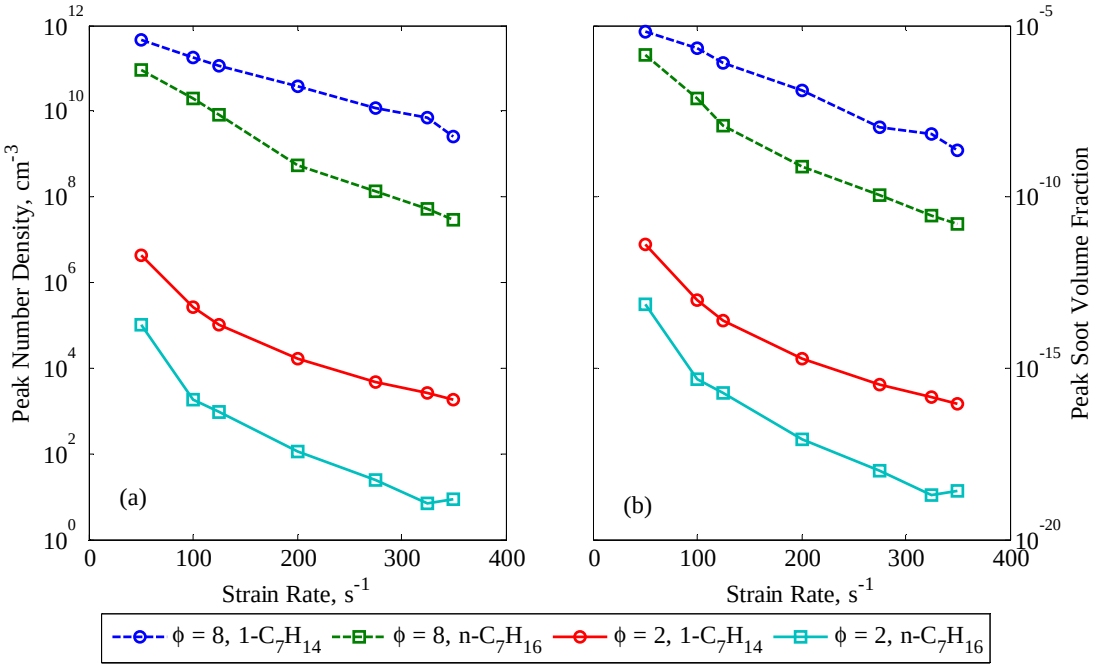

Figure 7: Peak particle number density (a) and soot volume fraction (b) plotted versus strain rate for n-heptane and 1-heptene PPFs at ϕ = 2 and 8.

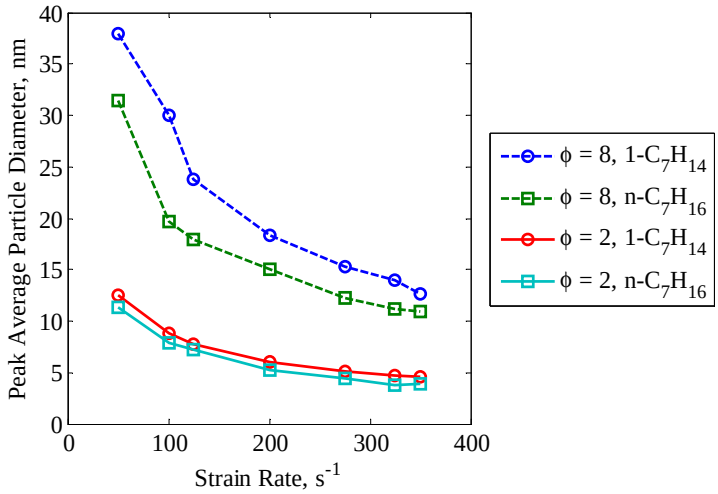

Figure 8: Peak average particle diameter plotted versus strain rate for n-heptane and 1-heptene PPFs at ϕ = 2 and 8.

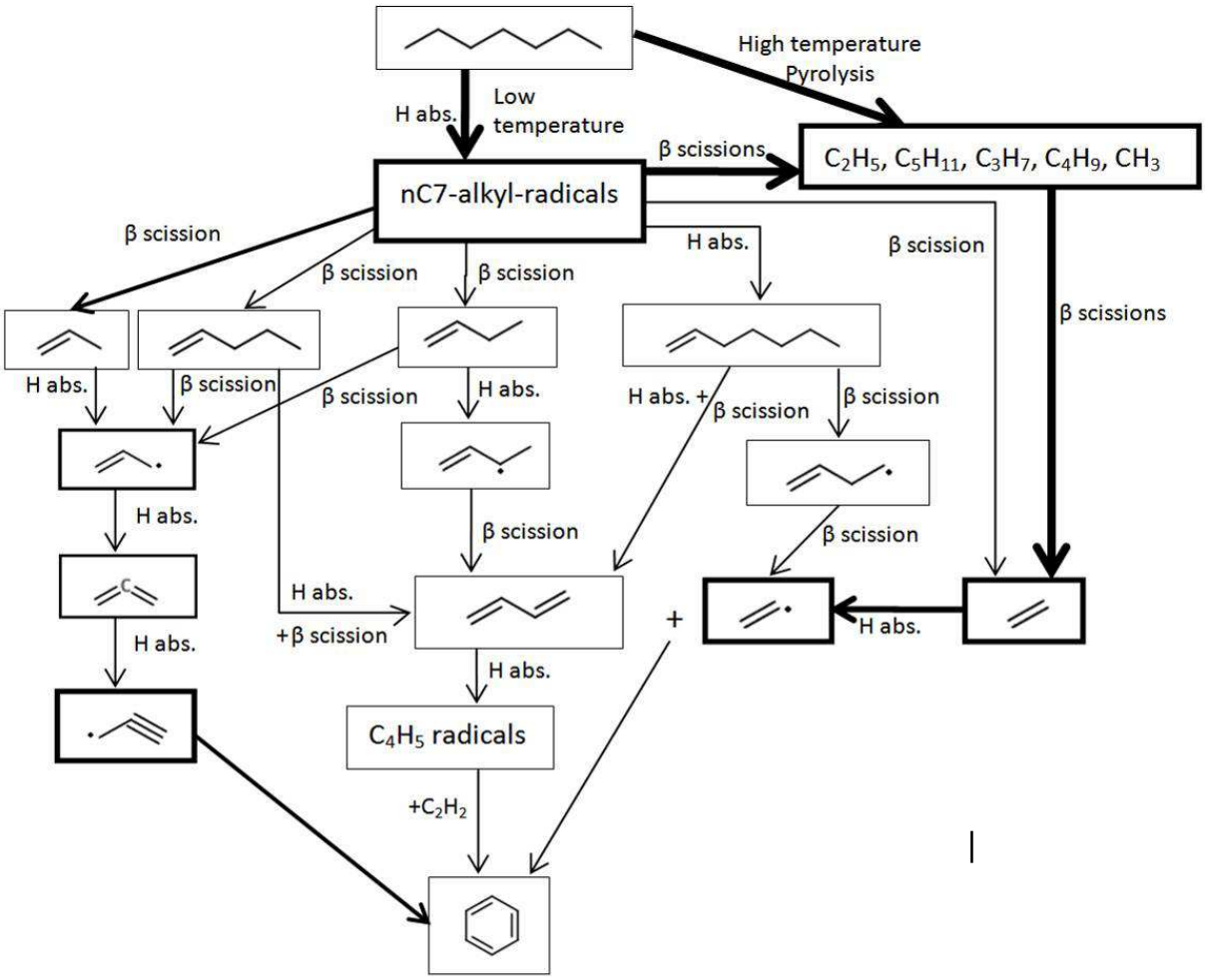
High temperature
Pyrolysis
H abs.
Low
temperature
β scissions
C_2H_5, C_5H_{11}, C_3H_7, C_4H_9, CH_3
nC7-alkyl-radicals
β scission
β scission
β scission
H abs.
β scission
β scissions
H abs.
β scission
H abs.
β scission
H abs. +
β scission
β scission
H abs.
β scission
H abs.
β scission
H abs.
+β scission
H abs.
+
H abs.
H abs.
C_4H_5 radicals
$+C_2H_2$

(a)

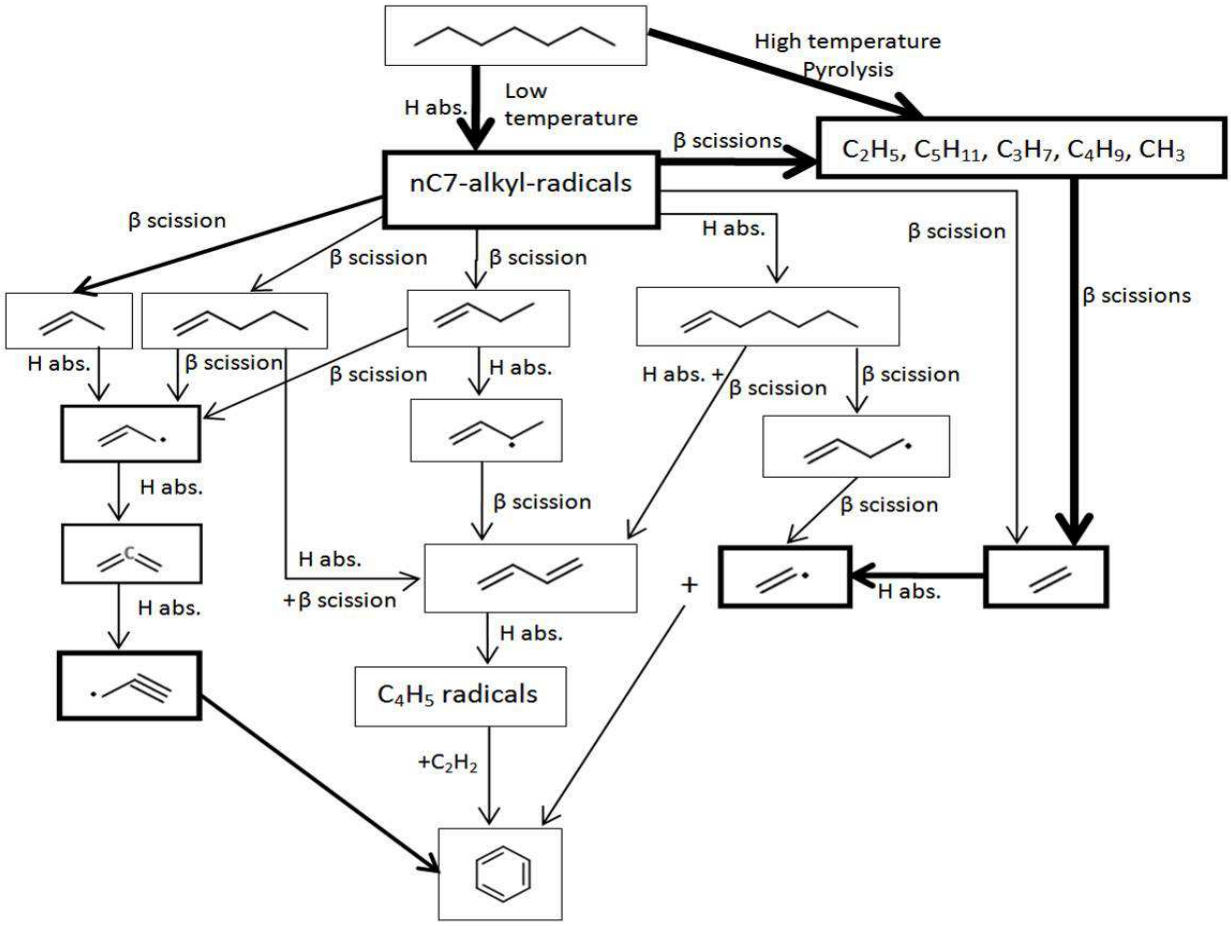

(b)

Figure 9: Benzene formation pathways in n-heptane (a) and 1-heptene (b) flames.